Am J Physiol Cell Physiol 302: C494–C504, 2012.
First published November 2, 2011; doi:10.1152/ajpcell.00267.2011.

T-type Ca^{2+} channels in mouse embryonic stem cells: modulation during cell cycle and contribution to self-renewal

José A. Rodríguez-Gómez,* Konstantín L. Levitsky,* and José López-Barneo

Instituto de Biomedicina de Sevilla; Hospital Universitario Virgen del Rocío/CSIC/Universidad de Sevilla, and Centro de Investigación Biomédica en Red sobre Enfermedades Neurodegenerativas, Seville, Spain

Submitted 29 July 2011; accepted in final form 27 October 2011

Rodríguez-Gómez JA, Levitsky KL, López-Barneo J. T-type Ca^{2+} channels in mouse embryonic stem cells: modulation during cell cycle and contribution to self-renewal. *Am J Physiol Cell Physiol* 302: C494–C504, 2012. First published November 2, 2011; doi:10.1152/ajpcell.00267.2011.—Ion channels participate in cell homeostasis and are involved in the regulation of proliferation and differentiation in several cell types; however, their presence and function in embryonic stem (ES) cells are poorly studied. We have investigated the existence of voltage-dependent inward currents in mouse ES cells and their ability to modulate proliferation and self-renewal. Patch-clamped ES cells had inactivating tetrodotoxin (TTX)-sensitive Na^+ currents as well as transient Ca^{2+} currents abolished by the external application of Ni^{2+}. Biophysical and pharmacological data indicated that the Ca^{2+} current is predominantly mediated by T-type ($Ca_v3.2$) channels. The number of cells expressing T-type channels and $Ca_v3.2$ mRNA levels increased at the G1/S transition of the cell cycle. TTX had no effect on ES cell proliferation. However, blockade of T-type Ca^{2+} currents with Ni^{2+} induced a decrease in proliferation and alkaline phosphatase positive colonies as well as reduced expression of Oct3/4 and Nanog, all indicative of loss in self-renewal capacity. Decreased alkaline phosphatase and Oct3/4 expression were also observed in cells subjected to small interfering RNA-induced knockdown for T-type ($Ca_v3.2$) Ca^{2+} channels, thus partially recapitulating the pharmacological effects on self-renewal. These results indicate that $Ca_v3.2$ channel expression in ES cells is modulated along the cell cycle being induced at late G1 phase. They also suggest that these channels are involved in the maintenance of the undifferentiated state of mouse ES cells. We propose that Ca^{2+} entry mediated by $Ca_v3.2$ channels might be one of the intracellular signals that participate in the complex network responsible for ES cell self-renewal.

voltage-dependent inward currents; proliferation; $Ca_v3.2$ channel expression

FOR THE LAST FEW YEARS embryonic stem (ES) cells have attracted the attention of numerous investigators due to their usefulness for developmental studies and because of their ability to differentiate in multiple cell classes with potential applicability to regenerative medicine. However, the basic physiological features of ES cells are poorly known. Mouse ES cells are derived from the inner cell mass of preimplantation embryos. In the presence of serum and leukemia inhibitory factor (LIF), these cells can self-renew, meaning that they proliferate maintaining an undifferentiated and pluripotent state (5, 47). Pluripotency is defined as the capacity to generate all the differentiated cell types that constitute the adult organism. It is known that propagation of ES cells in an undifferentiated state is governed by a complex interplay among a network of transcription factors, epigenetic processes, and intracellular messengers (35). However, complete elucidation of the mechanisms controlling ES cells self-renewal and pluripotency has not yet been achieved.

ES cells are thought to be nonexcitable, although their electrophysiological properties have not been thoroughly investigated. Voltage- and ligand-gated ion channels are known to exist in ES cells. In this regard, hyperpolarization-activated inward currents, outwardly rectifying K^+ currents, and GABA-activated chloride currents have been reported in mouse ES cells (1, 25, 49). Moreover, voltage-dependent K^+ currents can be also recorded from human ES and induced-pluripotent stem (iPS) cells (20). However, voltage-gated Na^+ and Ca^{2+} channels, although essential for numerous cell functions, have not been studied in detail in ES cells.

Voltage-gated Ca^{2+} channels are key players for regulated Ca^{2+} influx in cells (3, 7). Cytosolic Ca^{2+} concentration is a highly versatile intracellular variable that regulates a broad variety of cellular processes, including some of early stages of development, proliferation, differentiation, and apoptosis (42, 51). Ca^{2+} transients are known to occur at the awakening of quiescence, at the G1/S transition, during S-phase, and at the exit from mitosis (2, 44). In mouse ES cells Ca^{2+} oscillations have also been shown peaking at G1/S transition (22). There are two major classes of voltage-dependent Ca^{2+} channels: high-voltage activated (HVA) channels, which include the L-, N-, P/Q- and R-subtypes, and low-voltage activated (LVA), or T-type, channels (19, 41). In addition to their distinct voltage dependence of activation, T-type calcium channels also exhibit unique rapid inactivation and slow deactivation time course (41). The T-type channel family comprise three subtypes, namely $Ca_v3.1$, $Ca_v3.2$, and $Ca_v3.3$, which can be distinguished, among other features, by their sensitivity to Ni^{2+} (21, 26). The implication of T-type Ca^{2+} channels in mechanisms relevant for cell proliferation have been described in different tumor (for review see Ref. 40) and nontumor cells such as the single and two-cell mouse embryo (12), vascular smooth muscle (24, 43), newborn ventricular myocytes (17, 30), newborn chromaffin cells (29), preadipocytes (36), and myoblasts (4). Interestingly, in rat aortic smooth muscle cells T-type Ca^{2+} currents have been shown to change along the cell cycle, because this activity was present only at the G1 and S phases (24).

Altogether, these observations prompted us to evaluate whether ES cells express voltage-gated inward currents and, more specifically, if T-type Ca^{2+} channels participate in the physiology of these highly proliferating cells. Particularly, we

* J. A. Rodríguez-Gómez and K. L. Levitsky contributed equally to this work.

Address for reprint requests and other correspondence: J. López-Barneo, Instituto de Biomedicina de Sevilla, Campus Hospital Universitario Virgen del Rocío, Avda. Manuel Siurot, s/n, 41013 Seville, Spain (e-mail: lbarneo@us.es).

wanted to know whether T-type Ca^{2+} channels contribute to the maintenance of undifferentiated state of ES cells, or, contrarily, induce differentiation. Herein we show that T-type Ca^{2+} channels are functionally expressed in mouse ES cells and that cells expressing the $Ca_v3.2$ channel subtype are more abundant in the G1/S transition of the cell cycle. We also report by both pharmacological and small interfering RNA (siRNA) tools that Ca^{2+} entry mediated by T-type channels could play a role in preserving self-renewal capacity in mouse ES cells. We discuss these results in the context of the physiological regulation of ES cell cycle.

MATERIALS AND METHODS

ES cell culture, differentiation, and synchronization. Four mouse ES cell lines were used: AINV15, D3, IB10, and R1. R1 mouse ES cells were cultured in the presence of 1,400 U/ml of LIF (Millipore, Temecula, CA) and expanded by periodical passage in coculture with 10 μg/ml mitomycin C-inactivated (Roche Diagnostics) mouse embryonic fibroblasts to prevent differentiation (27). AINV15 and D3 mouse ES cell lines were cultured and expanded as R1 line with minor modifications in media composition (32). IB10 cells were cultured in medium with addition of buffalo rat liver cells-conditioned medium. R1 cells were used at passages 6, 7, 12, and 13. AINV15, D3, and IB10 cells were used at passages 22, 29, and 8, respectively. To block Ca^{2+} entry and to chelate Ca^{2+} in culture medium, nickel (II) chloride hexahydrate ($NiCl.6H_2O$, Sigma-Aldrich) and EGTA (Sigma-Aldrich) were applied respectively on ES cell culture for 12, 24, or 48 h. To block Na^+ channels tetrodotoxin (TTX, Sigma-Aldrich) was applied on ES cell culture for 12 h.

Cell-cycle synchronization in G1/S transition was performed in all ES cell lines studied as previously described (16). Briefly, cells were sequentially treated with 2.5 mM thymidine (Sigma-Aldrich), washed with PBS, and treated with 0.5 mM mimosine (Sigma-Aldrich). At this point cells were dissociated and processed either for electrophysiological, cell cycle, and mRNA expression analysis. For electrophysiological study, cells were replated on mimosine-containing medium for preservation of G1 blockade. Alternatively to mimosine, hydroxyurea (Sigma-Aldrich) was also used.

For expansion, cell-cycle blockade and pharmacological as well as siRNA treatments cells were cultured at high density (40,000–62,000 cells/cm^2) to minimize differentiation caused by low cell density. Cell density was maintained constant for each type of experiment.

Electrophysiology. Macroscopic Ca^{2+} and Na^+ currents were recorded using the whole cell configuration of the patch-clamp technique as adapted to our laboratory (13, 29). ES cell cultures were dissociated with trypsin to single-cell suspension and replated in slivers on poly-L-lysine-coated coverslips for electrophysiological recording 1 to 4 h later. In these conditions mouse embryonic fibroblasts, present in a much smaller number than ES cells, were clearly distinguishable by their larger size. All experiments were conducted at room temperature (22–25°C). For whole cell patch recordings, the internal solution contained (in mM) 110 CsCl, 30 CsF, 10 EGTA, 10 HEPES, and 4 ATP-Mg; pH was adjusted with CsOH to 7.2 and osmolality was 285 mosM/kg. The standard bath solution contained (in mM) 140 NaCl, 9 $BaCl_2$, 1 $CaCl_2$, 10 HEPES, and 10 glucose. pH was adjusted with NaOH to 7.4 and osmolality was 300 mosM/kg.

Cell cycle analysis. For analysis on DNA content, cells were fixed by 70% ethanol dropwise addition, rehydrated in PBS, and stained for propidium iodide with CycleTest PLUS DNA Reagent kit (Becton Dickinson, San Jose, CA). Fluorescence intensity was analyzed on a Cytomics flow cytometer (Beckman Coulter, Brea, CA). Data acquisition was performed using MXP software (Beckman Coulter), and the cell cycle pattern was analyzed with FlowJo software (Tree Star, Ashland, OR).

Immunofluorescence. For immunocytochemistry, cells were fixed with 4% paraformaldehyde/PBS for 20 min, washed in PBS, and then blocked for 1 h at room temperature with 10% normal donkey serum (NDS, Jackson ImmunoResearch Laboratories) and 1% of BSA (Sigma-Aldrich) in PBS. Next, cells were incubated with monoclonal mouse antibody against stage-specific embryonic antigen 1 (SSEA-1, 1/300, Developmental Studies Hybridoma Bank, University of Iowa) diluted in the blocking solution overnight at 4°C. Cells were washed the following day with 0.1% BSA-PBS, treated with permeabilization solution containing 0.1% Triton-10% NDS-1% BSA-PBS for 1 h at room temperature, and incubated with rabbit polyclonal $Ca_v3.2$ antibody (1/50, gift from Dr. Farach-Carson) diluted in the permeabilization solution overnight at 4°C. Next, cells were washed with 0.1% BSA-PBS, incubated with FITC donkey anti-mouse IgM (Jackson ImmunoResearch Laboratories) and Alexa 568 donkey anti-rabbit IgG (Molecular Probes, Eugene, OR) secondary antibodies, both at 1/400 for 1 h at room temperature and washed. To visualize nuclei, cells were also stained with 4′-6-diamidino-2-phenylindole (DAPI, 1/1,000, Sigma-Aldrich). Fluorescence was detected with a confocal microscope (TCS SP2, Leica, Germany).

For flow cytometry, cultured cells were dissociated, washed in PBS, and resuspended without fixation in staining solution containing (for 50 ml): 44 ml of L15 medium, 100 U/ml penicillin-100 mg/ml streptomycin, 10 mM HEPES (all from GIBCO), 0.1 g BSA, and 2.5 mM EDTA (Sigma-Aldrich). Next, cells were incubated with SSEA-1 antibody (1/300) for 30 min at 4°C and washed and incubated with FITC donkey anti-mouse IgM (1/400) for 30 min at 4° C. After final wash, cells were resuspended in 2 mg/ml 7-amino-actinomycin (7-AAD, Molecular Probes) to eliminate dead cells from analyses as 7-AAD+. Analyses were performed in a MoFlo three laser flow-cytometer (DAKO Cytomation, Fort Collins, CO).

Alkaline phosphatase assay. Cells were fixed in 4% paraformaldehyde-PBS for 1–2 min, and staining for alkaline phosphatase was performed at room temperature using an Alkaline Phosphatase Detection Kit (Millipore) containing Naphtol/Fast Red Violet Solution as recommended by the manufacturer. Colonies were observed under an inverted microscope (IX-71, Olympus, Japan), and the ratios of undifferentiated versus total number of colonies were scored. Undifferentiated colonies were considered as those with intense alkaline phosphatase staining and defined and tight boundaries.

Gene-expression analysis. Total RNA was isolated from ES cells using Nucleospin RNA II (Macherey-Nagel) with additional RNA precipitation. RNA samples (2–5 μg) were treated with DNase I (Invitrogen, Carlsbad, CA) and used to prepare first-strand cDNA using SuperScript II (Invitrogen). cDNA samples were subjected to conventional and real-time PCR amplification with specific primers. Real-time PCR was carried out using an ABI Prism 7500 Sequence Detection System (Applied-Biosystems, Foster City, CA) and SYBR Green PCR Master mix (Applied-Biosystems). In each sample 18S RNA levels were measured to normalize for RNA amounts and to perform relative quantifications. For both PCRs, analyses primers were designed using the Primer Express software (Applied-Biosystems). For conventional PCR the following primers were used for amplification of target mRNAs: Cacna1g ($Ca_v3.1$), forward 5′-TGGTGGTGGAGAACTTCCATA-3′ and reverse 5′-GAAGCAATTACATCGTCCAACA-3′; Cacna1h ($Ca_v3.2$), forward 5′-CCGCTATCTGTCCAACGAC-3′ and reverse 5′-TACCTTCTTACGCCAACGG-3′; Cacna1i ($Ca_v3.3$), forward 5′-GTGCCTCGTTGTCATAGCGAC-3′ and reverse 5′-TGGCCTTGCGAAGGATGT-3′. For real-time PCR the following primers were used for amplification of target mRNAs: Cacna1g, forward 5′-TGCTGTGGAAATGGTGGTGA-3′ and reverse 5′-AGCATCCCAGCAATGACGAT-3′; Cacna1h, forward 5′-TGAGCATGGGTGTTGAGTATCAT-3′ and reverse 5′-GGTGAACACGATGTTGCTTATCTC-3′; Cacna1i, forward 5′-GTGAACATCATGTATAATGGATTGGA-3′ and reverse 5′-TGTGGTTTGTCACCGGCTG-3′; Pou5f1 (Oct3/4), forward 5′-TCACATCGCCAATCAGCTTG-3′ and reverse 5′-GAACCATACTCGAACCACATCCTT-3′; Nanog, forward 5′-ACCAGTGGTTGAA-

GACTAGCAATG-3′ and reverse 5′-CTGGTGCTGAGCCCTTCTG-3′; 18s, forward 5′-AACGAGACTCTGGCATGCTAACTA-3′ and reverse 5′-GCCACTTGTCCCTCTAAGAAGT-3′.

RNA interference. Transient knockdowns of $Ca_v3.1$ and $Ca_v3.2$ channels were performed with siRNAs obtained from Ambion (Austin, TX). The target mRNA sequences for the siRNAs were the following: Cacna1g, sense GGAAGAUCGUAGAUAGCAAtt and antisense UUGCUAUCUACGAUCUUCCgg; Cacn1h, sense GGGCUUCCUUUAGUAGCAAtt and antisense UUGCUACUAAAGGAAGCCCag; sequence of scramble negative control siRNA was not provided. Optimization of ES cells transfection conditions was carried out by cells transfection with a cytomegalovirus-green fluorescent protein (GFP)-expressing plasmid and subsequent flow cytometry analysis of GFP-positive cells. The best results were obtained by cells transfection 6 h postplating at high cell density (62,000 cells/cm^2). GFP expression level reached a maximum at 2 days posttransfection (57% of GFP+ cells). ES cells were transfected with 20 or 40 nM of the siRNA duplex using RNAimax lipofectamine (Invitrogen) with previous conditions. siRNA-lipofectamine complexes were prepared in Opti-MEM I reduced-serum medium (GIBCO, Gaithersburg, MD). Cells were treated with siRNA-lipofectamine complexes, and 5 h later complexes were diluted twice with antibiotic-free medium and cultured for 2 days before RNA interference effects were evaluated. Knockdown results were obtained comparing $Ca_v3.1$ and $Ca_v3.2$ siRNA treatment with the corresponding dose of scramble negative control.

Estimation of Ca^{2+}-buffering capacity of the ES cell culture medium. To evaluate the divalent cation buffering capacity of the ES cells culture medium, which could provide some evidence on the chelation of Ni^{2+} by the same medium, we used a calcium electrode (Orion Calcium Electrode, Thermo). We added 1 mM Ca^{2+} to the standard solution provided by the manufacturer, which had an osmolality of 150 mosmol/kg. In these conditions the response of the electrode was lineal to added Ca^{2+} in the range between 0 and 300 μM. The ES cell culture medium, diluted to one-half to reach an osmolality similar to that of the standard solution, had an estimated free Ca^{2+} concentration ~1 mM. In these conditions the electrode was unresponsive to added calcium between 0 and 75 μM and only started to measure free added calcium with a lineal curve similar to the one observed with the standard solution, after adding Ca^{2+} at concentrations higher than 100 μM. These measurements indicate that even half-diluted ES cell culture medium, containing fetal bovine serum and other agents, has a clearly manifested capacity to chelate Ca^{2+} and possibly other divalent cations.

Statistical analysis. Values are given as means ± SE. The statistical significance of differences was analyzed using unpaired Student's *t*-test with SigmaStat software.

RESULTS

Inward Na^+ and Ca^{2+} currents in mouse ES cells. Most of our experiments were performed on R1 mouse ES cells. This preparation was composed mainly of undifferentiated cells since ~90% of them expressed SSEA-1 as analyzed by flow cytometry (Fig. 1*A*). We focused on the characterization of inward voltage-dependent ionic currents in ES cells. To this end, ES cells were dialyzed with Cs^+ as an ion for substitution of K^+ (13, 29), which abolishes outward voltage-gated K^+ currents described in these cells (13, 29).

We have distinguished four subpopulations of R1 ES cells subjected to whole cell patch clamp (step depolarization to +20 mV followed by repolarization to −70 mV), according to the characteristics of the inward currents that they exhibited

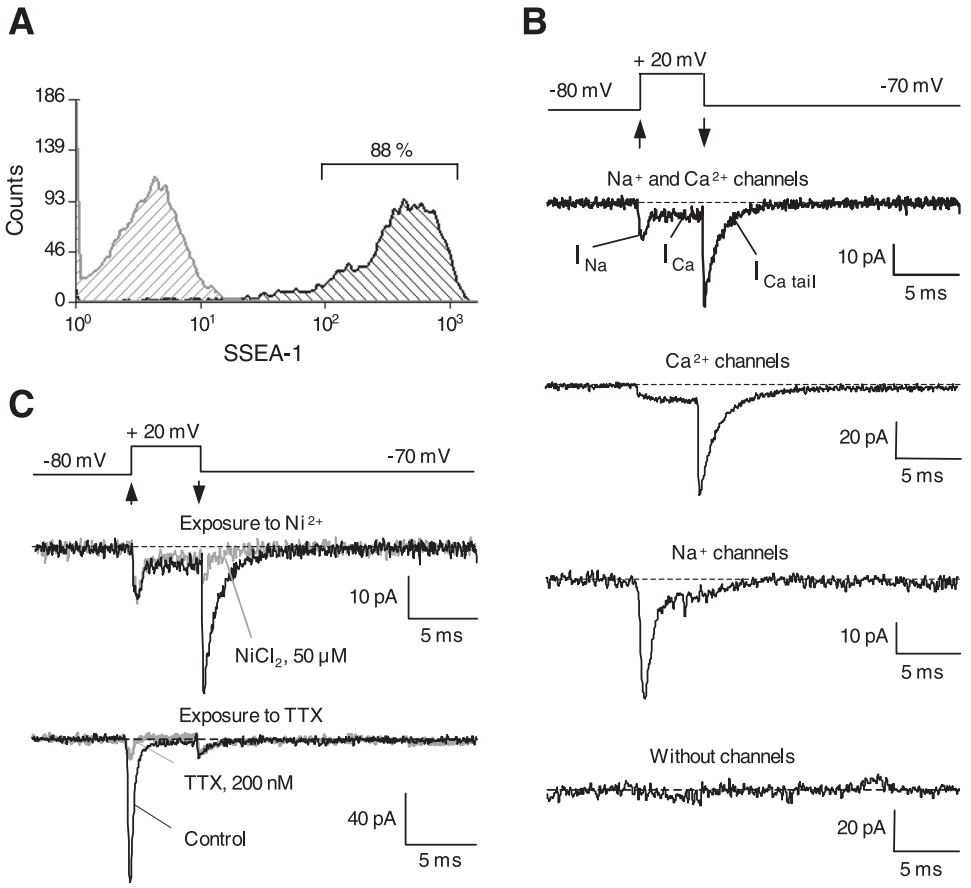

Fig. 1. Inward currents in mouse embryonic stem (ES) cells. *A*: flow cytometry analysis performed on mouse ES cells for stage-specific embryonic antigen-1 (SSEA-1, black line). As negative control cells were incubated in parallel without the corresponding primary antibody (gray line). *B*: representative examples of different macroscopic sodium (I_{Na}) and calcium (I_{Ca}) currents recorded in mouse ES cells subjected to whole cell patch clamp. *C*: selective inhibition of the Ca^{2+} tail current by external application of $NiCl_2$ (50 μM) is shown in the *top* (gray trace). Selective inhibition of the rapid Na^+ current by external application of tetrodotoxin (TTX, 200 nM) is shown in the *bottom* (gray trace). The current trace in *B* (*top*) is the same as in *C* (*top*).

(see Fig. 1*B* for representative examples). We have found cells that showed Na^+ and Ca^{2+} currents, only Ca^{2+} currents, only Na^+ currents, or no appreciable currents. The quantitative analysis given in Table 1 indicates that in normal conditions (asynchronous culture) many ES cells (~65%) had measurable inward currents mediated by Ca^{2+} and/or Na^+ ions. In cells expressing Na^+ and Ca^{2+} currents the calcium tail current was reversibly abolished by application to the external solution of 50 μM Ni^{2+}, which at this concentration selectively blocks T-type (α_{1H}) Ca^{2+} channels (26) (Fig. 1*C*, *top*). Note that no effect was observed on the Na^+ current. In cells expressing Na^+ channels, the fast sodium current was reversibly blocked by 200 nM TTX, a well-known specific Na^+ channel blocker (Fig. 1*C*, *bottom*).

The identification of Ca^{2+} currents in mouse ES cells as T-type was confirmed by their rapid inactivation, a distinct feature of LVA against HVA Ca^{2+} channels (41). Figure 2, *A* and *B*, shows representative examples of the deactivating Ca^{2+} currents recorded in R1 mouse ES cells upon repolarization to −70 mV after a depolarizing pulse to +20 mV lasting either 5 ms (short pulse) or 50 ms (long pulse). The recordings clearly indicate that the component of the tail current present at the end of 5 ms pulse disappeared almost completely at the end of the 50-ms pulse, suggesting inactivation of the T-type channels during the maintained depolarization. This test was performed in every cell exhibiting Ca^{2+} current. A slow component in the deactivation, or closing, tail current (indicated by arrow in Fig. 2*C*, *left*) was consistently observed, further suggesting the presence of a population of T-type Ca^{2+} channels that are known to close about ~10–20 times more slowly than either Na^+ or HVA Ca^{2+} channels (13, 31). To further characterize the calcium tail currents evoked upon repolarization, we estimated the closing time constant (τ) by fitting an exponential function to the deactivating segment of the current (Fig. 2*C*, *right*). The deactivating currents were well fitted by a single exponential function with a time constant that at −70 mV averaged 1.46 ± 0.11 ms (see Table 1). This deactivation time constant is similar to that reported for native and recombinant T channels of the $Ca_v3.2$ subtype expressing the α_{1H} subunit (13, 31). T-type Ca^{2+} currents of similar kinetics were recorded in R1 ES cells at earlier passage as well as in other mouse ES cell lines (Table 2; see also below). These observations suggest that mouse ES cells posses a significant population of voltage-dependent Na^+ and Ca^{2+} channels. The Ca^{2+} current shows typical kinetics of fast inactivating and slowly deactivating T-type channels. The data also indicate that the Ca^{2+} channels present in mouse ES cells predominantly belong to the $Ca_v3.2$ subtype.

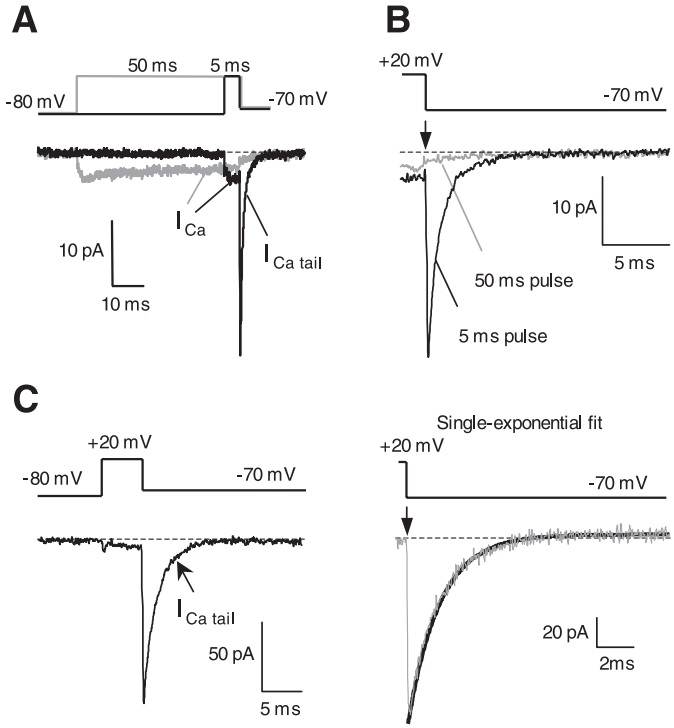

Fig. 2. T-type Ca^{2+} channels in mouse ES cells. *A*: calcium currents from mouse ES cells during short- (black) and long- (gray) lasting depolarizing pulses. *B*: Ca^{2+} tail currents after short and long pulses at an expanded time scale. Note the disappearance of the tail generated at the end of 50-ms pulses (gray trace) due to inactivation of the T-type channels. *C*: *left*, example of calcium currents recorded in mouse ES cells. *Right*, Ca^{2+} tail currents at an expanded time base. Fitting by a single-exponential function (black line) is shown superimposed on the current trace (gray). No fast component was observed.

$Ca_v3.2$ T-type Ca^{2+} channels are induced at G1/S transition in mouse ES cells. Pharmacological blockade of the cell cycle was used to study whether T-type Ca^{2+} channel expression is modified during ES cell cycle and whether they are preferentially expressed in cells at G1/S transition (24). We used a double blocking strategy consisting in arresting cells at G2/M phase by thymidine application followed by mimosine treatment to arrest them at late G1 phase (16, 50). Mimosine has been described as a cell cycle blocker arresting cells just at the very end of G1 phase, since DNA replication occurs within 15 min of releasing cells from the mimosine block (23). This manipulation of the cell cycle rendered an accumulation of cells in G1/S transition observed by an increase of cells in G1

Table 1. *Electrical parameters and inward ionic currents in asynchronous and G1-synchronized R1 mouse ES cells*

Parameter	Asynchronous Cells	G1-Synchronized Cells
$I_{Ca} + I_{Na}$, %	11.1 ($n = 45$)	34.3 ($n = 67$)
I_{Ca}, %	35.6 ($n = 45$)	38.8 ($n = 67$)
t_{deact}, ms (at −70 mV)	1.46 ± 0.11 ($n = 24$)	1.49 ± 0.06 ($n = 50$)
I_{Ca}, pA/pF (at +20 mV)	4.12 ± 1.19 ($n = 24$)	5.49 ± 0.57 ($n = 50$)
I_{Na}, %	17.8 ($n = 45$)	4.5 ($n = 67$)
I_{Na}, pA/PF (at +20 mV)	3.70 ± 0.68 ($n = 13$)	4.40 ± 0.60 ($n = 26$)
No channels, %	35.5 ($n = 45$)	22.4 ($n = 67$)
Cell capacitance, pF	5.77 ± 0.17 ($n = 45$)	5.94 ± 0.13 ($n = 67$)

Values of electrical parameters are means ± SE; *n*, number of cells in parentheses. $I_{Ca} + I_{Na}$, percentage of cells with inward Na^+ and/or Ca^{2+} currents, respectively; pA/pF: current density; t_{deact}: time constant of deactivation.

Table 2. *Comparison of T-type calcium currents in different mouse ES cell lines*

Cell Line	I_{Ca}, %	t_{deact}, ms (at −70 mV)
R1 (P13)	46.7 ($n = 45$)	1.46 ± 0.11
R1 (P6)	45.4 ($n = 11$)	1.39 ± 0.05
AINV15	47.5 ($n = 19$)	1.98 ± 0.15
D3	27.3 ($n = 11$)	1.03 ± 0.13
IB10	9.3 ($n = 43$)	1.59 ± 0.14

Values are means ± SE; *n*, number of cells in parentheses.

phase (25% vs. 52%) and a decrease in S phase (58% vs. 36%) when asynchronous and G1-synchronized cultures were compared (Fig. 3*A*, *left* and *right*, respectively). Changes of Ca^{2+} channel expression along the cell cycle are shown in Fig. 3*B*. In G1-synchronized cultures the proportion of cells without Ca^{2+} channels was lower than in asynchronous cells (27% vs. 53%, respectively). Correspondingly, the proportion of cells presenting Ca^{2+} currents was higher in G1-arrested condition than in the asynchronous one (73% vs. 47%, respectively). Despite the increase in the number of G1-arrested cells expressing Ca^{2+} channels, no changes were observed either in cell size (estimated by measuring cell capacitance) or in calcium current density. The time constant of T-type current deactivation was also unaltered (see Table 1).

To check whether the increase in number of cells with Ca^{2+} channels was a cell cycle-related event or rather an artifactual phenomenon caused by mimosine acting directly on the channels, we synchronized the cells in G1/S transition using hydroxyurea, another G1-arresting agent, instead of mimosine. In this condition, a similar profile of change in proportions of cells with and without Ca^{2+} channels was obtained (data not shown).

As a test of the undifferentiated state of the cells during cell cycle arrest, expression of markers of ES cell pluripotency, Oct3/4, and Nanog was examined by real-time PCR on asynchronous and G1-synchronized cells. Oct3/4 and Nanog mRNA levels increased, 11 and 14%, respectively, in G1-synchronized cells but we can think of this slight induction as a transient change in gene expression along cell cycle progression (data not shown). Mimosine-induced G1 blockade was fully reversible and after washing out the drug the normal cell cycle profile of asynchronous cells was reestablished in G1-arrested cells after an 8-h culture period (data not shown), as it was previously observed (23).

The molecular nature of the T-type channel class expressed in ES cells as well as its regulation during cell cycle were further analyzed by conventional and real-time PCR. In asynchronous cells we amplified mRNA of the three T-type channels subtypes (Fig. 3*C*). Their relative expression levels estimated on real-time PCR data were 0.63 ± 0.05, 0.36 ± 0.05, and 0.01 ± 0.01 ($n = 4$) for $Ca_v3.1$, $Ca_v3.2$, and $Ca_v3.3$, respectively. In G1-arrested cells, $Ca_v3.2$ mRNA levels increased significantly (~1.7-fold), but the expression of the other two channel types remained unchanged (Fig. 3*D*). These results suggest that although both $Ca_v3.1$ and $Ca_v3.2$ mRNAs appear to be abundant in mouse ES cells, the $Ca_v3.2$ subtype is the predominant channel contributing to the T-type Ca^{2+} current. Molecular and biophysical data indicate that this channel class is selectively upregulated at the G1/S transition of the cell cycle. Localization of $Ca_v3.2$ channel in the plasma membrane was observed by immunocitochemistry in SSEA-1-positive R1 ES cells (Fig. 4).

To ascertain whether the presence of T-type Ca^{2+} channels is a general property of ES cells, we recorded ionic currents from several ES cell lines growing in asynchronous state. A representative example is shown in Fig. 5*A*. Although the percentage of cells presenting Ca^{2+} channels varied in the different ES lines studied (AINV15, D3, and IB10), they all seemed to have electrophysiologically similar T-type Ca^{2+} currents (Table 2). The deactivation time constant characteris-

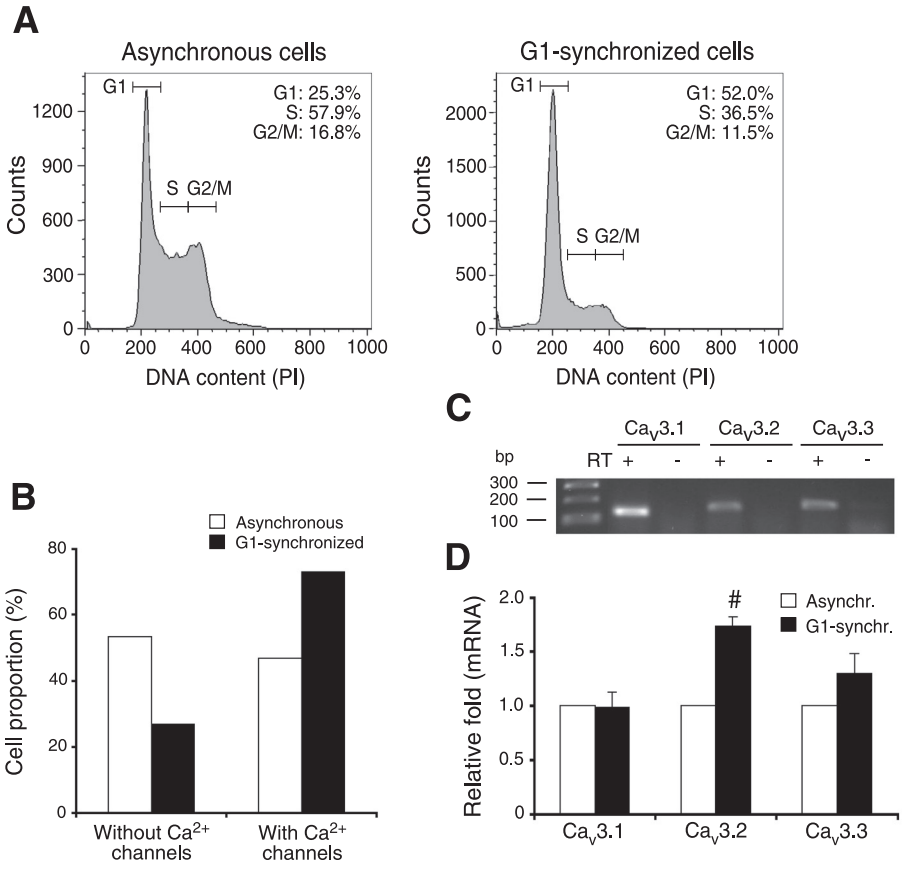

Fig. 3. T-type Ca^{2+} channels are active at G1/S transition of the cell cycle. *A*: cell cycle analysis of mouse ES cells in asynchronous condition (*left*) and after G1 synchronization (*right*). *B*: number of cells with and without Ca^{2+} currents in asynchronous ($n = 45$) and G1-arrested ($n = 67$) cells. Both cell types were counted in five independent experiments of cell cycle synchronization and divided by the number of total cells. *C*: expression of T-type Ca^{2+} channels transcripts in ES cells analyzed by conventional PCR. Molecular size of the standards is shown on *left*. Reverse transcription control was performed on RNA sample without SuperScritpt II enzyme (RT-). *D*: gene expression levels of T-type Ca^{2+} channels in asynchronous and G1-arrested cells analyzed by real-time PCR. The graph represents the mean values ± SE ($n = 4$). #$P < 0.01$.

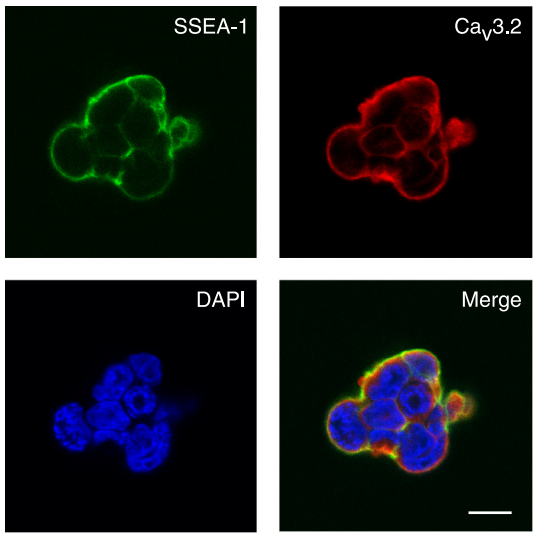

Fig. 4. Immunocytochemical analysis of mouse ES cells for SSEA-1 and $Ca_v3.2$ channel expression. Scale bar, 10 μm.

tic of T-type Ca^{2+} channels was approximately the same in all cell lines. No major electrophysiological differences were either observed in T-type Ca^{2+} currents between R1 ES cells at different passage (Table 2). We also studied T-type Ca^{2+} channel mRNA expression in AINV15, D3, and IB10 cells. As in R1 cells (see Fig. 3*C*), the three Ca_v3 channel types were detected in these ES lines (Fig. 5*B*). Quite interestingly, the relative expression levels of the various Ca_v3 channel types were almost the same as those described above for R1 cells. Relative expression levels for Cav3.1, Cav 3.2, and Cav.3.3, respectively, were 0.62 ± 0.06, 0.34 ± 0.05, and 0.04 ± 0.01, (n = 3) for AINV15; 0.60 ± 0.07, 0.36 ± 0.07, and 0.04 ± 0.01 (n = 3) for D3; and 0.75 ± 0.04, 0.22 ± 0.05, and 0.03 ± 0.01 (n = 3) for IB10 cells. Expression of T-type Ca^{2+} channels after cell cycle arrest at G1/S transition was also studied in AINV15, D3, and IB10 cells. Cell cycle blockade was performed using the same protocol as for R1 cells (data not shown). Analysis of the two most abundant channels ($Ca_v3.1$ and $Ca_v3.2$.) indicated that, as in R1 cells, synchronization of the three ES lines resulted in selective increase in mRNA expression of $Ca_v3.2$ channels (Fig. 5*C*). These data suggest that T-type Ca^{2+} channel expression and their modulation along the cell cycle are intrinsic properties of mouse ES cell lines.

Pharmacological blockade of T-type Ca^{2+} channels impairs self-renewal of mouse ES cells. As we found that $Ca_v3.2$ expression is modulated during the cell cycle, we sought whether inhibition of T-type Ca^{2+} channels activity would have an effect on proliferation and maintenance of the undifferentiated state of ES cells. Ni^{2+} has been demonstrated to be an effective blocker of heterologously expressed recombinant T-type Ca^{2+} channels with higher affinity for $Ca_v3.2$ than for $Ca_v3.1$ channels (21). Therefore, we studied R1 ES cells treated with increasing concentrations of Ni^{2+} during 12 h since their cell cycle is estimated to last for ~10–12 h. For comparison, we also studied the effect of extracellular Ca^{2+} chelation by addition of 5 mM EGTA. The effect on cell proliferation of Ca^{2+} channel blockade and Ca^{2+} chelation was evaluated by cell counting after Trypan blue exclusion. Ni^{2+} application (300 μM) and EGTA addition caused significant decreases in cell number (Fig. 6*A*). To precisely evaluate the proliferation effect of Ni^{2+} and EGTA, the cell cycle pattern was analyzed by propidium iodide staining followed by flow cytometry (Fig. 6*B*). We observed that Ni^{2+} at 150 and 300 μM caused a significant decrease of cells in the S phase, suggesting a decrease in the proliferation rate, and a small, but significant, increase of cells in sub-G1 phase, probably indicative of an apoptotic process. No change was found in the percentage of cells in the G1 phase at the Ni^{2+} concentrations

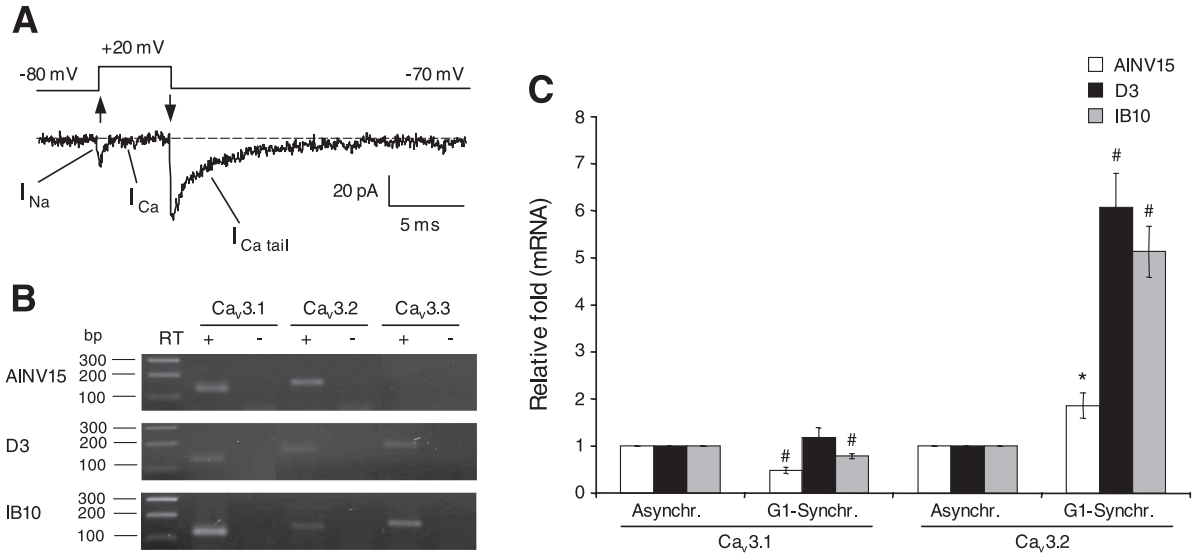

Fig. 5. T-type Ca^{2+} channels are induced in different ES cell lines at G1/S transition of the cell cycle. *A*: representative example of macroscopic sodium (I_{Na}) and calcium (I_{Ca}) currents recorded in AINV15 ES cell line subjected to whole cell patch clamp. Note the slow time course of the deactivation current ($I_{Ca\ tail}$) typical of T-type Ca^{2+} channels. *B*: expression of T-type Ca^{2+} channel transcripts in AINV15, D3, and IB10 ES cell lines analyzed by conventional PCR. Molecular size of the standards is shown on the *left*. Reverse transcription control was performed on RNA sample without SuperScritpt II enzyme (RT-). *C*: gene expression levels of T-type Ca^{2+} channels in asynchronous and G1-arrested AINV15, D3, and IB10 ES cells analyzed by real-time PCR. The graph represents the mean values ± SE (n = 3). *$P < 0.05$, #$P < 0.01$.

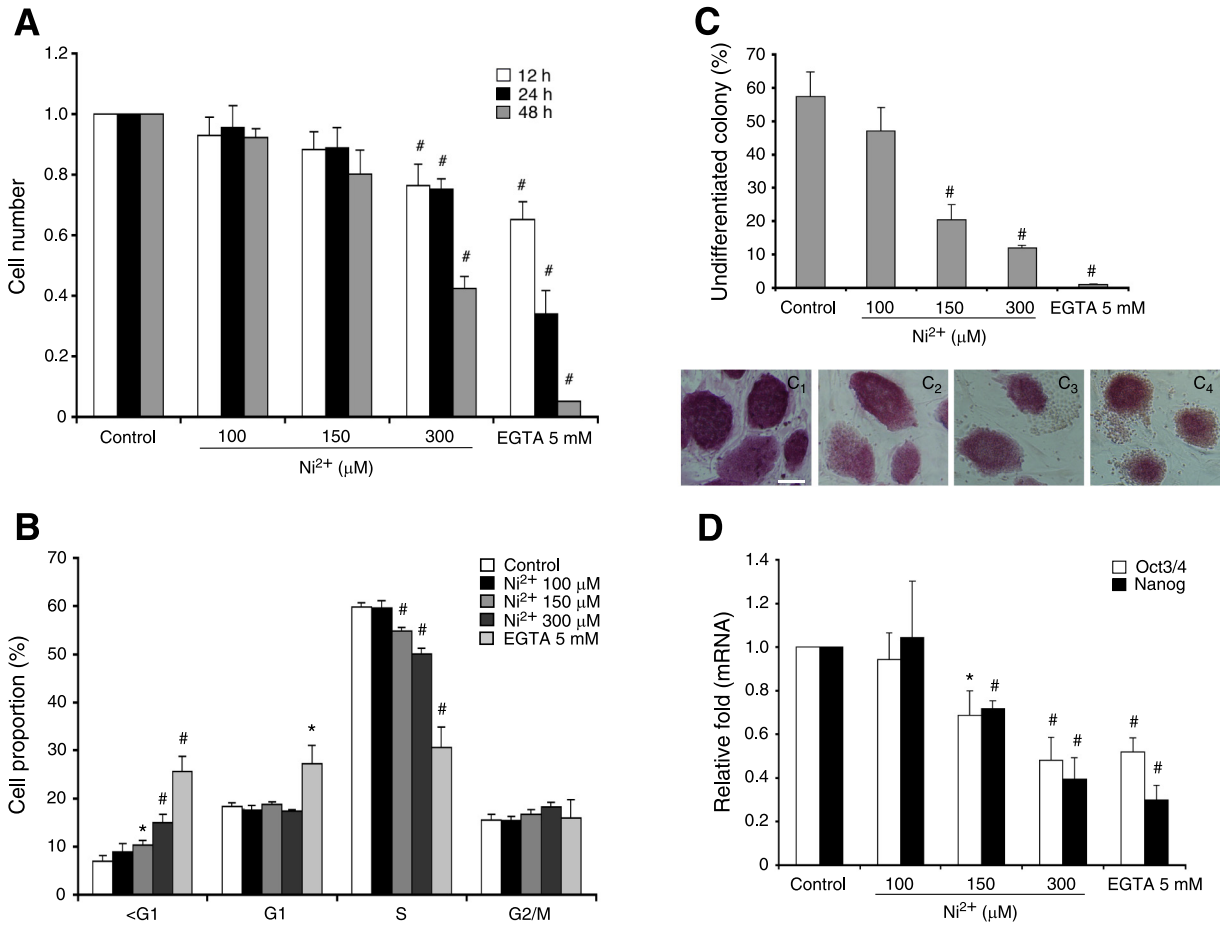

Fig. 6. Ni^{2+} treatment impairs self-renewal of mouse ES cells. *A*: quantification of cells treated with increasing doses of Ni^{2+} and a Ca^{2+} chelant, EGTA (5 mM) for 12, 24, and 48 h. The graph represents means ± SE ($n = 6$). #$P < 0.01$. *B*: cell cycle analysis of ES cells treated for 12 h with increasing doses of Ni^{2+} and EGTA (5 mM). The graph represents the means ± SE ($n = 6$). *$P < 0.05$, #$P < 0.01$. *C*: analysis of alkaline phosphatase activity on ES cells exposed to increasing doses of Ni^{2+} and EGTA (5 mM) for 12 h. The graph represents the means ± SE ($n = 4$). #$P < 0.01$. Representative fields of cells of control (C_1), Ni^{2+} 150 μM (C_2), Ni^{2+} 300 μM (C_3), and EGTA 5 mM (C_4) conditions and stained for alkaline phosphatase are shown (*bottom*). Scale bar, 50 μM. *D*: gene expression levels of ES cells markers Oct3/4 and Nanog in ES cells treated with increasing doses of Ni^{2+} and EGTA (5 mM) for 12 h. Analysis was performed by real-time PCR. The graph represents the means ± SE ($n = 4$). *$P < 0.05$, #$P < 0.01$.

used. Meanwhile, EGTA clearly induced a more potent cell cycle arrest and cell death process, as we found a significant decrease of cells in S phase and increase for sub-G1 and G1 fractions. Difference between Ni^{2+} and EGTA effects on cell cycle pattern underlines the subtle change on cell proliferation provoked by Ca^{2+} channels blockade compared with Ca^{2+} chelation. The magnitude of changes provoked by exposure to Ni^{2+} and Ca^{2+} chelation on cell proliferation increased when the treatment was expanded from 12 h to 24 or 48 h, possibly due to prolonged differentiation and cell death (Fig. 6*A*). Since we observed an increased presence of Na^+ channels in G1/S synchronized cells (see Table 1), we studied the effect of Na^+ channel blockade (TTX was applied at 200 and 500 nM during 12 h) on proliferation. No significant changes were observed in any of the phases of the cell cycle, thus suggesting that Na^+ channels do not significantly participate in cell proliferation (data not shown).

Self-renewal of Ni^{2+}- and EGTA-treated ES cells in the 12-h time point was evaluated by alkaline phosphatase activity assay and real-time PCR of pluripotency marker genes Oct3/4 and Nanog. Ni^{2+} application (at 150 and 300 μM) caused significant decreases in the number of alkaline phosphatase-positive undifferentiated colonies (Fig. 6*C*). EGTA had a stronger effect and led to almost abolishment of the presence of undifferentiated colonies. Similarly, mRNA levels of Oct3/4 and Nanog were downregulated by Ni^{2+} (at 150 and 300 μM), as well as by EGTA treatment (Fig. 6*D*). Taken together, these results suggest that blockade of T-type Ca^{2+} channels decreases proliferation and self-renewal of mouse ES cells.

RNA interference of $Ca_v3.2$ channels induce ES cell differentiation. To assess specifically the role of T-type Ca^{2+} channels on ES self-renewal an RNA interference assay was performed with siRNA expression plasmids for $Ca_v3.1$ and $Ca_v3.2$, the most abundantly expressed T-type Ca^{2+} channels in ES cells. Interference efficiency was tested by real-time PCR of the target gene in cells transfected with scramble negative control, $Ca_v3.1$, and $Ca_v3.2$ siRNAs (Fig. 7*A*). After transfection with siRNA for $Ca_v3.1$ at 40 nM, mRNA level of the target gene was reduced to 25%, whereas $Ca_v3.2$ mRNA levels were nonspecifically decreased to 75% of control values. Meanwhile, siRNA for $Ca_v3.2$ at 20 and 40 nM reduced expression levels of the target gene to 43% and 40%, respectively. $Ca_v3.2$ siRNA treatment also caused a nonspecific decrease in mRNA levels of $Ca_v3.1$ channels. Downregulation of $Ca_v3.1$ and $Ca_v3.2$ mRNA caused no signifi-

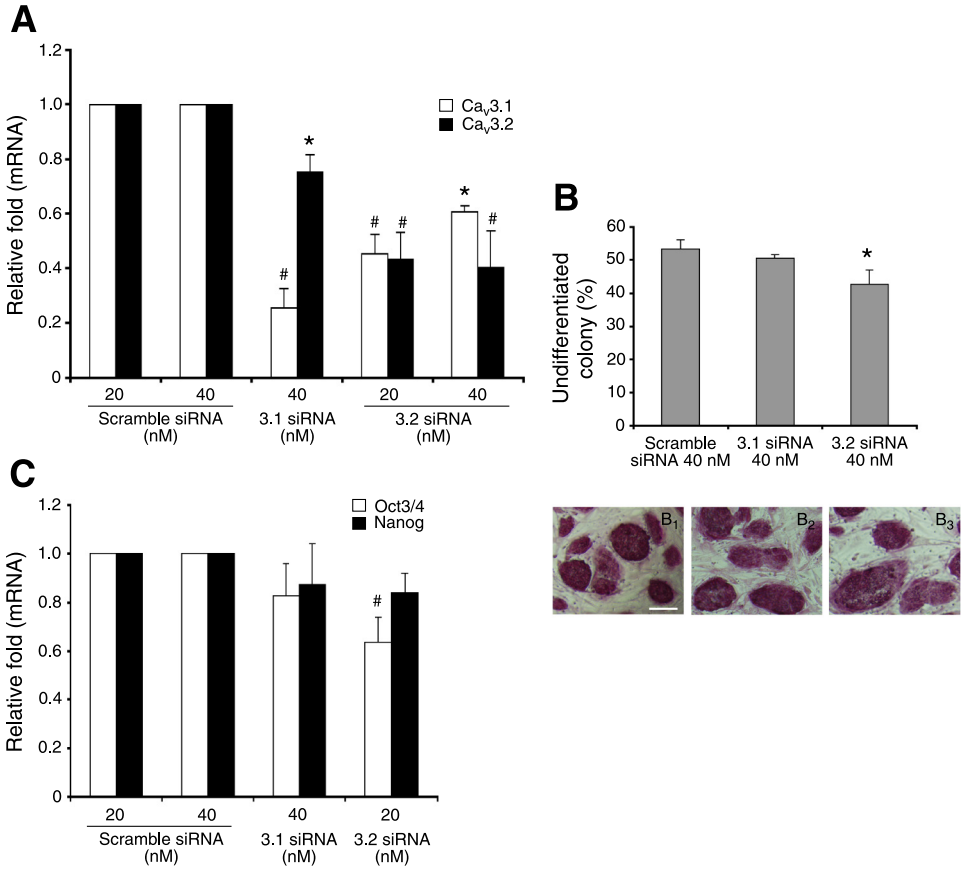

Fig. 7. RNA interference of $Ca_v3.2$ induces differentiation of mouse ES cells. *A*: gene expression levels of $Ca_v3.1$ and $Ca_v3.2$ genes in cells treated with scramble negative control (at 20 and 40 nM), $Ca_v3.1$ at 40 nM, and $Ca_v3.2$ (at 20 and 40 nM) small interfering RNA (siRNAs). Analysis was performed by real-time PCR. The graph represents the means ± SE ($n = 4$). *$P < 0.05$, #$P < 0.01$. *B*: analysis of alkaline phosphatase activity in mouse ES cells treated with scramble negative control, $Ca_v3.1$, and $Ca_v3.2$ siRNAs all at 40 nM. The graph represents the means ± SE ($n = 4$). *$P < 0.05$. Representative fields of cells treated with 40 nM scramble negative control (B_1), $Ca_v3.1$ (B_2), and $Ca_v3.2$ siRNAs (B_3) and stained for alkaline phosphatase are shown (*bottom*). Scale bar, 50 μM. *C*: gene expression levels of ES cells markers Oct3/4 and Nanog treated with scramble negative control (at 20 and 40 nM), $Ca_v3.1$ at 40 nM and $Ca_v3.2$ siRNAs at 20 nM. Analysis was performed by real-time PCR. The graph represents the means values ± SE ($n = 4$). #$P <$ 0.01.

cant change in cell growth or cell cycle pattern of siRNA-treated cells (data not shown). However, the percentage of alkaline phosphatase-positive undifferentiated colonies decreased significantly for cells transfected with 40 nM $Ca_v3.2$ siRNA but not for 40 nM $Ca_v3.1$ siRNA transfection (Fig. 7*B*). Expression levels of ES cell markers were reduced significantly for Oct3/4 but not for Nanog in cells transfected with 20 nM $Ca_v3.2$ siRNA (Fig. 7*C*). Slight decreases in both genes were found in cells treated with 40 nM $Ca_v3.1$ siRNA, but none of them reached significance. These results support the view that T-type current attributed to $Ca_v3.2$ channels is participating in the mechanism responsible of maintenance of mouse ES cells self-renewal.

DISCUSSION

The electrophysiological properties of ES cells are poorly defined, hence, this report aimed at the characterization of the inward currents present in these cells. Membrane ion channels play fundamental roles in a myriad of cellular processes, including proliferation and differentiation. We have found that several lines of undifferentiated mouse ES cells have voltage-dependent Ca^{2+} and/or Na^+ currents. Molecular and electrophysiological evidence indicate that the Ca^{2+} currents are almost exclusively mediated by LVA or T-type Ca^{2+} channels. We show that T-type channels are modulated along cell cycle progression and contribute to maintenance of ES cells self-renewal. ES cell self-renewal, which is widely defined as promotion of proliferation accompanied by suppression of differentiation (5, 47), is required in order that pluripotency is retained. Detailed characterization of the signaling pathways operating in self-renewal and pluripotency will contribute to exploit the full potential of ES cells.

ES cells are known to express outward K^+ currents and hyperpolarization-activated inward currents (49), but to our knowledge, this is the first report where functional voltage-gated Ca^{2+} and Na^+ channels were recorded in these cells. In a recent paper (46), mRNA of various Ca^{2+} channel classes (L, N, R, and T) were amplified by PCR from preparations of mouse ES cells; however, whether these mRNAs are translated to functional channels was not analyzed. In the current study, we have shown that among the various classes of HVA or LVA Ca^{2+} channels, only T-type channels are indeed functional in the mouse ES cell lines studied. The deactivation time course and sensitivity to Ni^{2+} suggest that of the three T-type mRNA species amplified by PCR, $Ca_v3.2$ channels (α_{1H} subunit) are the main contributors to the Ca^{2+} current in mouse ES cells (21, 26, 31). We also found several electrophysiologically distinct subpopulations of undifferentiated ES cells depending on whether they express Na^+ channels, Ca^{2+} channels, both, or none of them. Although the functional role of the Na^+ currents was not studied in detail, Ca^{2+} channel function seems to be associated with maintenance of proliferation and undifferentiated state of the cells.

Blockade of T-type Ca^{2+} channel with Ni^{2+} (at 150 and 300 μM) during 12 h was sufficient to decrease proliferation rate and provoke a substantial loss in R1 ES cells self-renewal, observed as reduction in the percentage of undifferentiated colonies, and decreased expression of pluripotency markers Oct3/4 and Nanog. Ni^{2+} application induced moderate de-

crease of cells in S phase, which is an indication of elevated ES cell differentiation (45, 52). On the other hand, increase in sub-G1 fractions at 150 and 300 μM Ni^{2+} could be indicative of apoptotic cell death, an event also associated to blastocyst development and LIF withdrawal-induced mouse ES cell differentiation (10, 15, 33, 39). Alternatively, apoptosis could be caused by toxicity induced by Ni^{2+} exposure (6). It is important to note that the differentiation effect induced by Ni^{2+} was only clearly observed at concentrations an order of magnitude higher than those required to selectively block recombinant $Ca_v3.2$ channels (IC_{50} ~5–10 μM) (21). It is therefore possible that native $Ca_v3.2$ channels expressed in ES cells have lower apparent affinity for Ni^{2+} than the heterologously expressed channels. An additional circumstance that could explain the relatively high Ni^{2+} concentrations required to alter ES cell self-renewal is that free Ni^{2+} concentration could be less than the presumed nominal value due to divalent cation chelation by components (such as fetal bovine serum) of the ES cell culture medium. Indeed, a powerful Ca^{2+}-chelating capacity of the culture medium was observed (see MATERIALS AND METHODS).

In accord with the pharmacological data, $Ca_v3.2$ siRNA treatment induced a modest, but statistically significant, loss of self-renewal observed as a decrease in the percentage of undifferentiated colonies and Oct3/4 mRNA expression level. Because of the lower changes in the undifferentiated state, the proliferation capacity of ES cells remained unchanged. The relatively moderate effect of $Ca_v3.2$ knockdown on ES self-renewal compared with Ni^{2+} application can be explained by the limited efficiency of siRNA to inhibit the $Ca_v3.2$ transcript (60% reduction of mRNA expression). It is also noteworthy that in parallel experiments $Ca_v3.1$ knockdown did not cause any significant change on the self-renewal parameters of ES cells.

The most plausible role of T-type Ca^{2+} channels in ES cells is to regulate transmembrane Ca^{2+} influx, which could, in turn, influence the expression of the gene program, or signaling pathways necessary for proliferation and self-renewal. The particular biophysical features of T-type Ca^{2+} channels allow them to open at membrane potentials slightly more negative than those at which they fully inactivate. In a membrane potential range near the cell resting potential there is a small percentage of channels that are not inactivated and can mediate small sustained inward Ca^{2+} currents ("window currents") (9, 11). Therefore, in ES cells T-type Ca^{2+} channels could translate subtle changes in membrane potential into modifications of transmembrane Ca^{2+} influx and increase of cytosolic Ca^{2+} concentration. Indeed, it is known that membrane potential is a critical factor for cell cycling as blockade of K^+ channel activity leads to membrane depolarization, arrest in early G1, and decreased proliferation rate in different cell types, including mouse ES cells and human iPS cells (20, 34, 38, 49, 53–55). The role of intracellular Ca^{2+} oscillations at the G1/S transition and proliferation has been highlighted in mouse ES cells (22). This last study reported that extracellular Ca^{2+} does not seem necessary for instauration of Ca^{2+} oscillations but for the maintenance of their amplitude, since oscillation was triggered by release of Ca^{2+} from endoplasmic reticulum in an inositol 1,4,5-trisphosphate-mediated mode. We have observed that $Ca_v3.2$ channels are upregulated at the G1/S transition, therefore, it is likely that Ca^{2+} influx mediated by T-type channels influence the amplitude of intracellular Ca^{2+} oscillations as cells progress from G1 to S phase. This can be particularly important for cell cycle regulation since it has been proven that the amplitude and duration of Ca^{2+} signals determine the activation of specific transcriptional pathways (14).

Mouse ES cells are characterized by extraordinarily rapid proliferation rate, primarily owing to a reduction in the duration of G1 phase of the cell cycle. Defining features of G1 phase in ES cells are constitutive cyclinE-CDK2 activity and hyperphosphorylated retinoblastoma protein (37). Increased intracellular Ca^{2+} level has been demonstrated to oscillate at different time points of the cell cycle including the G1/S transition (2, 44). Different signaling pathways could involve T-type Ca^{2+} channels as plausible cell cycle regulators in ES cells at G1/S transition. T-type Ca^{2+} currents have been shown mediating phenotype switching of nonproliferative to proliferative smooth muscle cells, and calmodulin, an intracellular calcium receptor, has been shown to participate in this transition (18). Calmodulin has also been demonstrated to facilitate G1/S transition in vascular smooth muscle cells via binding to cyclinE and possibly activating CDK2 (8). A different pathway would involve calmodulin as an inducer of retinoblastoma protein phosphorylation (48). Either by modulating constitutive cyclinE-CDK2 activity or by maintaining retinoblastoma hyperphosphorylation T-type Ca^{2+} channels activity could facilitate the transition from G1 to S phase in ES cells.

In conclusion, we show a novel feature of ES cells, which is the presence of Na^+ and T-type Ca^{2+} currents, the last ones mediated by $Ca_v3.2$ channels upregulated in the G1/S transition of the cell cycle. These channels seem to participate in the maintenance of the undifferentiated state of mouse ES cells. Taking into account that hypoxia induces $Ca_v3.2$ channels in cultured cells (13), it would be interesting to test whether the effect described here operates also in human ES and iPS cells considering that hypoxia maintains pluripotency of human ES cells and improves efficiency of adult cell reprogramming (28, 56). Further studies on the mechanisms linking ion channel activity, cell cycle regulation, and transcriptional networks may improve our understanding of ES cells self-renewal and pluripotency.

ACKNOWLEDGMENTS

Monoclonal $Ca_v3.2$ antibody was a kind gift of Dr. Mary C. Farach-Carson (Univ. of Delaware). We thank Dr. Juan Tejedo (Cabimer, Sevilla) for kindly providing AINV15 and D3 ES cell lines, Dr. Carmen Saez (Instituto de Biomedicina de Sevilla) for helping us to establish cell cycle synchronization experiments, and to Tree Star for kindly providing us free utilization of FlowJo software.

GRANTS

This research was supported by the Andalusian Government, Spanish Ministry of Science and Health and Marcelino Botín Foundation.

DISCLOSURES

No conflicts of interest, financial or otherwise, are declared by the author(s).

AUTHOR CONTRIBUTIONS

Author contributions: J.A.R.-G., K.L.L., and J.L.-B. conception and design of research; J.A.R.-G. and K.L.L. performed experiments; J.A.R.-G., K.L.L., and J.L.-B. analyzed data; J.A.R.-G., K.L.L., and J.L.-B. interpreted results of experiments; J.A.R.-G. and K.L.L. prepared figures; J.A.R.-G. and J.L.-B. drafted manuscript; J.A.R.-G., K.L.L., and J.L.-B. edited and revised manuscript; J.A.R.-G., K.L.L., and J.L.-B. approved final version of manuscript.

REFERENCES

1. **Andang M, Hjerling-Leffler J, Moliner A, Lundgren TK, Castelo-Branco G, Nanou E, Pozas E, Bryja V, Halliez S, Nishimaru H, Wilbertz J, Arenas E, Koltzenburg M, Charnay P, El Manira A, Ibanez CF, Ernfors P.** Histone H2AX-dependent GABA(A) receptor regulation of stem cell proliferation. *Nature* 451: 460–464, 2008.
2. **Berridge MJ.** Calcium signalling and cell proliferation. *Bioessays* 17: 491–500, 1995.
3. **Berridge MJ, Bootman MD, Roderick HL.** Calcium signalling: dynamics, homeostasis and remodelling. *Nat Rev Mol Cell Biol* 4: 517–529, 2003.
4. **Bijlenga P, Liu JH, Espinos E, Haenggeli CA, Fischer-Lougheed J, Bader CR, Bernheim L.** T-type alpha 1H Ca^{2+} channels are involved in Ca2+ signaling during terminal differentiation (fusion) of human myoblasts. *Proc Natl Acad Sci USA* 97: 7627–7632, 2000.
5. **Burdon T, Smith A, Savatier P.** Signalling, cell cycle and pluripotency in embryonic stem cells. *Trends Cell Biol* 12: 432–438, 2002.
6. **Caicedo M, Jacobs JJ, Reddy A, Hallab NJ.** Analysis of metal ion-induced DNA damage, apoptosis, and necrosis in human (Jurkat) T-cells demonstrates Ni2+ and V3+ are more toxic than other metals: Al^{3+}, Be^{2+}, Co^{2+}, Cr^{3+}, Cu^{2+}, Fe^{3+}, Mo^{5+}, Nb^{5+}, Zr^{2+}. *J Biomed Mater Res A* 86: 905–913, 2008.
7. **Catterall WA, Perez-Reyes E, Snutch TP, Striessnig J.** International Union of Pharmacology. XLVIII Nomenclature and structure-function relationships of voltage-gated calcium channels. *Pharmacol Rev* 57: 411–425, 2005.
8. **Choi J, Chiang A, Taulier N, Gros R, Pirani A, Husain M.** A calmodulin-binding site on cyclin E mediates Ca^{2+}-sensitive G1/s transitions in vascular smooth muscle cells. *Circ Res* 98: 1273–1281, 2006.
9. **Cohen CJ, McCarthy RT, Barrett PQ, Rasmussen H.** Ca channels in adrenal glomerulosa cells: K^+ and angiotensin II increase T-type Ca channel current. *Proc Natl Acad Sci USA* 85: 2412–2416, 1988.
10. **Coucouvanis E, Martin GR.** BMP signaling plays a role in visceral endoderm differentiation and cavitation in the early mouse embryo. *Development* 126: 535–546, 1999.
11. **Crunelli V, Toth TI, Cope DW, Blethyn K, Hughes SW.** The "window" T-type calcium current in brain dynamics of different behavioural states. *J Physiol* 562: 121–129, 2005.
12. **Day ML, Johnson MH, Cook DI.** Cell cycle regulation of a T-type calcium current in early mouse embryos. *Pflügers Arch* 436: 834–842, 1998.
13. **Del Toro R, Levitsky KL, Lopez-Barneo J, Chiara MD.** Induction of T-type calcium channel gene expression by chronic hypoxia. *J Biol Chem* 278: 22316–22324, 2003.
14. **Dolmetsch RE, Lewis RS, Goodnow CC, Healy JI.** Differential activation of transcription factors induced by Ca^{2+} response amplitude and duration. *Nature* 386: 855–858, 1997.
15. **Duval D, Malaise M, Reinhardt B, Kedinger C, Boeuf H.** A p38 inhibitor allows to dissociate differentiation and apoptotic processes triggered upon LIF withdrawal in mouse embryonic stem cells. *Cell Death Differ* 11: 331–341, 2004.
16. **Fujii-Yamamoto H, Kim JM, Arai K, Masai H.** Cell cycle and developmental regulations of replication factors in mouse embryonic stem cells. *J Biol Chem* 280: 12976–12987, 2005.
17. **Guo W, Kamiya K, Kodama I, Toyama J.** Cell cycle-related changes in the voltage-gated Ca^{2+} currents in cultured newborn rat ventricular myocytes. *J Mol Cell Cardiol* 30: 1095–1103, 1998.
18. **House SJ, Potier M, Bisaillon J, Singer HA, Trebak M.** The non-excitable smooth muscle: calcium signaling and phenotypic switching during vascular disease. *Pflügers Arch* 456: 769–785, 2008.
19. **Huc S, Monteil A, Bidaud I, Barbara G, Chemin J, Lory P.** Regulation of T-type calcium channels: signalling pathways and functional implications. *Biochim Biophys Acta* 1793: 947–952, 2009.
20. **Jiang P, Rushing SN, Kong CW, Fu J, Lieu DK, Chan CW, Deng W, Li RA.** Electrophysiological properties of human induced pluripotent stem cells. *Am J Physiol Cell Physiol* 298: C486–C495, 2010.
21. **Kang HW, Park JY, Jeong SW, Kim JA, Moon HJ, Perez-Reyes E, Lee JH.** A molecular determinant of nickel inhibition in Cav3.2 T-type calcium channels. *J Biol Chem* 281: 4823–4830, 2006.
22. **Kapur N, Mignery GA, Banach K.** Cell cycle-dependent calcium oscillations in mouse embryonic stem cells. *Am J Physiol Cell Physiol* 292: C1510–C1518, 2007.
23. **Krude T.** Mimosine arrests proliferating human cells before onset of DNA replication in a dose-dependent manner. *Exp Cell Res* 247: 148–159, 1999.
24. **Kuga T, Kobayashi S, Hirakawa Y, Kanaide H, Takeshita A.** Cell cycle-dependent expression of L- and T-type Ca^{2+} currents in rat aortic smooth muscle cells in primary culture. *Circ Res* 79: 14–19, 1996.
25. **Lau YT, Wong CK, Luo J, Leung LH, Tsang PF, Bian ZX, Tsang SY.** Effects of hyperpolarization-activated cyclic nucleotide-gated (HCN) channel blockers on the proliferation and cell cycle progression of embryonic stem cells. *Pflügers Arch* 461: 191–202, 2011.
26. **Lee JH, Gomora JC, Cribbs LL, Perez-Reyes E.** Nickel block of three cloned T-type calcium channels: low concentrations selectively block alpha1H. *Biophys J* 77: 3034–3042, 1999.
27. **Lee SH, Lumelsky N, Studer L, Auerbach JM, McKay RD.** Efficient generation of midbrain and hindbrain neurons from mouse embryonic stem cells. *Nat Biotechnol* 18: 675–679, 2000.
28. **Lengner CJ, Gimelbrant AA, Erwin JA, Cheng AW, Guenther MG, Welstead GG, Alagappan R, Frampton GM, Xu P, Muffat J, Santagata S, Powers D, Barrett CB, Young RA, Lee JT, Jaenisch R, Mitalipova M.** Derivation of pre-X inactivation human embryonic stem cells under physiological oxygen concentrations. *Cell* 141: 872–883, 2010.
29. **Levitsky KL, Lopez-Barneo J.** Developmental change of T-type Ca^{2+} channel expression and its role in rat chromaffin cell responsiveness to acute hypoxia. *J Physiol* 587: 1917–1929, 2009.
30. **Li M, Zhang M, Huang L, Zhou J, Zhuang H, Taylor JT, Keyser BM, Whitehurst RM Jr.** T-type Ca^{2+} channels are involved in high glucose-induced rat neonatal cardiomyocyte proliferation. *Pediatr Res* 57: 550–556, 2005.
31. **McRory JE, Santi CM, Hamming KS, Mezeyova J, Sutton KG, Baillie DL, Stea A, Snutch TP.** Molecular and functional characterization of a family of rat brain T-type calcium channels. *J Biol Chem* 276: 3999–4011, 2001.
32. **Mora-Castilla S, Tejedo JR, Hmadcha A, Cahuana GM, Martin F, Soria B, Bedoya FJ.** Nitric oxide repression of Nanog promotes mouse embryonic stem cell differentiation. *Cell Death Differ* 17: 1025–1033, 2010.
33. **Murray P, Edgar D.** Regulation of programmed cell death by basement membranes in embryonic development. *J Cell Biol* 150: 1215–1221, 2000.
34. **Ng SY, Chin CH, Lau YT, Luo J, Wong CK, Bian ZX, Tsang SY.** Role of voltage-gated potassium channels in the fate determination of embryonic stem cells. *J Cell Physiol* 224: 165–177, 2010.
35. **Niwa H.** How is pluripotency determined and maintained? *Development* 134: 635–646, 2007.
36. **Oguri A, Tanaka T, Iida H, Meguro K, Takano H, Oonuma H, Nishimura S, Morita T, Yamasoba T, Nagai R, Nakajima T.** Involvement of CaV3.1 T-type calcium channels in cell proliferation in mouse preadipocytes. *Am J Physiol Cell Physiol* 298: C1414–C1423, 2010.
37. **Orford KW, Scadden DT.** Deconstructing stem cell self-renewal: genetic insights into cell-cycle regulation. *Nat Rev Genet* 9: 115–128, 2008.
38. **Ouadid-Ahidouch H, Le Bourhis X, Roudbaraki M, Toillon RA, Delcourt P, Prevarskaya N.** Changes in the K^+ current-density of MCF-7 cells during progression through the cell cycle: possible involvement of a h-ether-a-gogo K^+ channel. *Receptors Channels* 7: 345–356, 2001.
39. **Pampfer S, Donnay I.** Apoptosis at the time of embryo implantation in mouse and rat. *Cell Death Differ* 6: 533–545, 1999.
40. **Panner A, Wurster RD.** T-type calcium channels and tumor proliferation. *Cell Calcium* 40: 253–259, 2006.
41. **Perez-Reyes E.** Molecular physiology of low-voltage-activated t-type calcium channels. *Physiol Rev* 83: 117–161, 2003.
42. **Rizzuto R, Pinton P, Ferrari D, Chami M, Szabadkai G, Magalhaes PJ, Di Virgilio F, Pozzan T.** Calcium and apoptosis: facts and hypotheses. *Oncogene* 22: 8619–8627, 2003.
43. **Rodman DM, Reese K, Harral J, Fouty B, Wu S, West J, Hoedt-Miller M, Tada Y, Li KX, Cool C, Fagan K, Cribbs L.** Low-voltage-activated (T-type) calcium channels control proliferation of human pulmonary artery myocytes. *Circ Res* 96: 864–872, 2005.
44. **Santella L.** The role of calcium in the cell cycle: facts and hypotheses. *Biochem Biophys Res Commun* 244: 317–324, 1998.
45. **Savatier P, Lapillonne H, van Grunsven LA, Rudkin BB, Samarut J.** Withdrawal of differentiation inhibitory activity/leukemia inhibitory

factor up-regulates D-type cyclins and cyclin-dependent kinase inhibitors in mouse embryonic stem cells. *Oncogene* 12: 309–322, 1996.
46. **Schwirtlich M, Emri Z, Antal K, Mate Z, Katarova Z, Szabo G.** GABA(A) and GABA(B) receptors of distinct properties affect oppositely the proliferation of mouse embryonic stem cells through synergistic elevation of intracellular Ca(2+). *FASEB J* 24: 1218–1228, 2010.
47. **Smith AG.** Embryo-derived stem cells: of mice and men. *Annu Rev Cell Dev Biol* 17: 435–462, 2001.
48. **Takuwa N, Zhou W, Kumada M, Takuwa Y.** Ca(2+)-dependent stimulation of retinoblastoma gene product phosphorylation and p34cdc2 kinase activation in serum-stimulated human fibroblasts. *J Biol Chem* 268: 138–145, 1993.
49. **Wang K, Xue T, Tsang SY, Van Huizen R, Wong CW, Lai KW, Ye Z, Cheng L, Au KW, Zhang J, Li GR, Lau CP, Tse HF, Li RA.** Electrophysiological properties of pluripotent human and mouse embryonic stem cells. *Stem Cells* 23: 1526–1534, 2005.
50. **Watson PA, Hanauske-Abel HH, Flint A, Lalande M.** Mimosine reversibly arrests cell cycle progression at the G1-S phase border. *Cytometry* 12: 242–246, 1991.
51. **Webb SE, Miller AL.** Calcium signalling during embryonic development. *Nat Rev Mol Cell Biol* 4: 539–551, 2003.
52. **White J, Stead E, Faast R, Conn S, Cartwright P, Dalton S.** Developmental activation of the Rb-E2F pathway and establishment of cell cycle-regulated cyclin-dependent kinase activity during embryonic stem cell differentiation. *Mol Biol Cell* 16: 2018–2027, 2005.
53. **Wonderlin WF, Strobl JS.** Potassium channels, proliferation and G1 progression. *J Membr Biol* 154: 91–107, 1996.
54. **Wonderlin WF, Woodfork KA, Strobl JS.** Changes in membrane potential during the progression of MCF-7 human mammary tumor cells through the cell cycle. *J Cell Physiol* 165: 177–185, 1995.
55. **Woodfork KA, Wonderlin WF, Peterson VA, Strobl JS.** Inhibition of ATP-sensitive potassium channels causes reversible cell-cycle arrest of human breast cancer cells in tissue culture. *J Cell Physiol* 162: 163–171, 1995.
56. **Yoshida Y, Takahashi K, Okita K, Ichisaka T, Yamanaka S.** Hypoxia enhances the generation of induced pluripotent stem cells. *Cell Stem Cell* 5: 237–241, 2009.